Final Technical Report for Award G15AP00067 (UCR) and G15AP00068 (UMass)

Dynamic models of potential earthquakes in the San Gorgonio Pass Region: Collaborative Research with University of California – Riverside and University of Massachusetts – Amherst

David D. Oglesby
Department of Earth Sciences
University of California, Riverside
Riverside, CA 92521-0423
PH: (951) 827-2036
FAX: (951) 827-4324
david.oglesby@ucr.edu

Michele L Cooke
Department of Geosciences
University of Massachusetts - Amherst
611 North Pleasant St.
Amherst, MA 01003-9297
PH: (413) 577-3142
FAX: (413) 545-1200
cooke@geo.umass.edu

Term covered: 05/01/2015-04/30/2017

Abstract

We use 3D dynamic finite element models to investigate potential rupture paths of earthquakes propagating along faults in the western San Gorgonio Pass (SGP) region, a structurally complex area along the San Andreas fault system (SAF) in southern California. We focus on the San Bernardino strand of the SAF, the San Gorgonio Pass Fault Zone, and a portion of the Garnet Hill strand of the SAF. The San Bernardino and Garnet Hill strands are predominately right-lateral strike-slip faults, while thrust faults dominate the San Gorgonio Pass Fault Zone, with small right-lateral tear faults between the thrust faults. We use the finite element method code FaultMod (Barall, 2009) to model rupture propagation and slip along a meshed fault geometry that reflects most of the surface trace complexity, and is consistent with long-term loading and observed surface deformation. We test three different types of pre-stress assumptions: 1) constant tractions, 2) regional stress regimes, and 3) long-term (evolved) stress from quasi-static three-dimensional crustal deformation modeling. The quasi-static model simulates long-term loading of the regional active fault network and the evolved stress state from this model considers stress accumulation along locked faults since the last earthquake rupture on each fault segment. Models with constant tractions assume pure right-lateral strike-slip motion on the San Bernardino and Garnet Hill strands and oblique thrust/right-lateral strike-slip motion on the San Gorgonio Pass Fault Zone. We find that the complexity of the fault geometry inhibits rupture propagation for several nucleation location and stress field assumptions, which may have implications for the reduced likelihood of through-going earthquakes scenarios along the SAF in southern California.

REPORT

1 Background

The San Gorgonio Pass (SGP) is located between the San Bernardino and San Jacinto mountains in southern California. In this region, the San Andreas Fault system (SAF) does not appear to have obviously continuous faults based on mapped surface traces (Figure 1). Faults appear discontinuous, and many of the relationships among the various mapped traces are unclear (Allen, 1957; Matti et al., 1985; Matti and Morton, 1993; Yule and Sieh, 2003). This is an important region in southern California seismology because of the uncertainty about its ability to produce large, through-going earthquakes. The entirety of the southern SAF, especially through the SGP, has not ruptured in modern, seismically recordable history, but if it were to fail in a single, through-going rupture, large parts of southern California could experience strong shaking (Olsen et al., 2006; 2008).

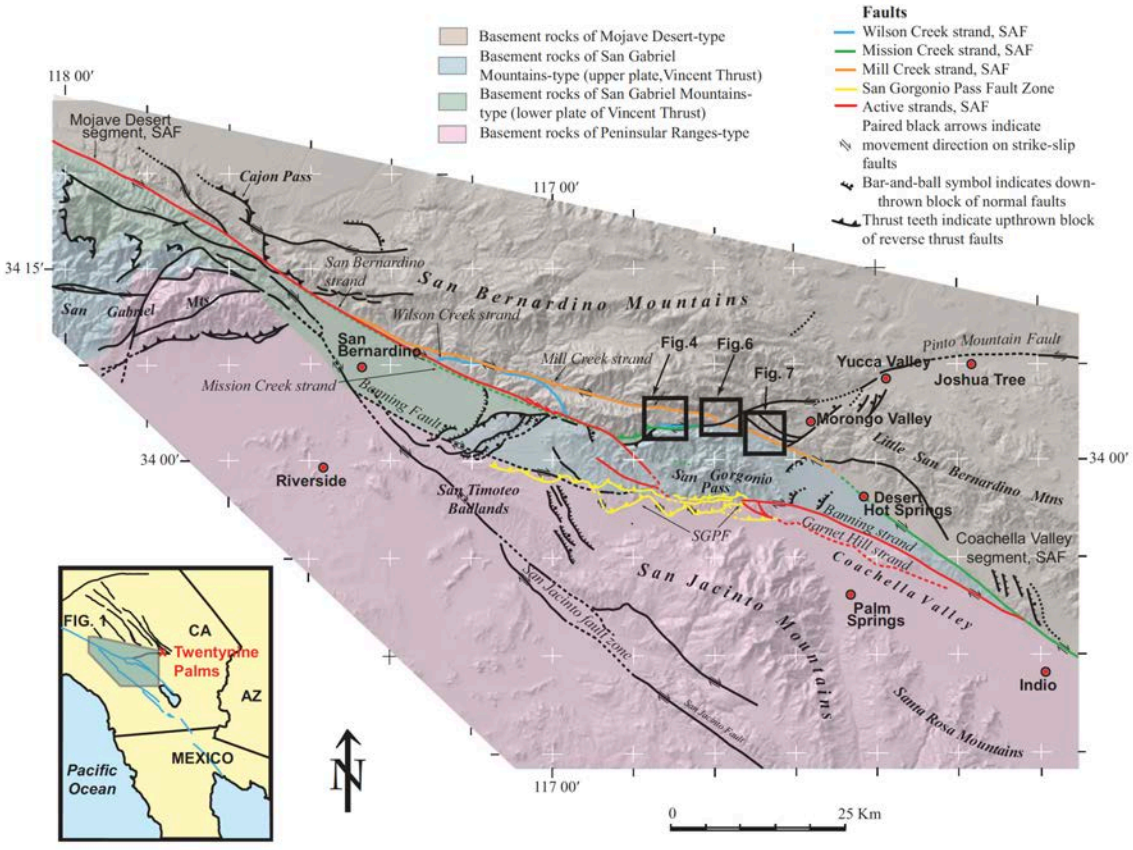

Figure 1. Geologic Map of Key Faults in the SGP. All annotations are original to the figure, from Kendrick et al. (2015). Original mapping from Matti et al., (1982) and Matti and Morton, (1993).

The SGP has a complex history of right-lateral strike-slip faulting, fault strand-switching, and convergence. The Mill Creek strand of the SAF is the most prominent through-going feature in the region, but it is deemed currently inactive (Matti et al., 1992; Kendrick et al., 2015). Many researchers have hypothesized that following the shut-off of the Mill Creek strand, the complexity of fault interactions in the SGP increased as less mechanically optimal paths to transfer slip developed (Matti et al., 1992; Yule and Sieh, 2003; Yule, 2009; Cooke and Dair, 2011; Kendrick *et al*., 2015). However, the Mill Creek strand is often still incorporated into

regional fault geometries such as the Southern California Earthquake Center (SCEC) Community Fault Model (Plesch *et al*., 2007) and the Uniform California Earthquake Rupture Forecast, Version 3 (UCERF3) (Field *et al.*, 2015). Modelers tend to favor simple structures in studies of hypothetical earthquake scenarios, and consequently several studies use simplified geometries that actually represent older, potentially inactive structures in the SGP (e.g., Meade and Hager, 2005; Smith and Sandwell, 2006; Olsen *et al*., 2006; Olsen *et al*., 2008). Quasi-static deformation models have tested various fault geometries through the SGP to see which geometries matched well with slip rate and uplift studies. Using an active Mill Creek strand did not produce a good match with the slip rate and uplift data (Dair and Cooke, 2009; Beyer et al., in review). Geologic mapping and paleoseismic studies indicate that thrust faults south of the San Bernardino Mountains (Figure 1) are likely some of the currently active structures (Allen, 1957; Matti *et al*., 1985; Yule and Sieh, 2003; Kendrick *et al.,* 2011; Ramzan, 2012, Scharer *et al*., 2013). Three-dimensional crustal deformation models that incorporate geometrically complex active thrust faults within the SGP (Cooke and Dair, 2011; Herbert and Cooke, 2012; Beyer et al., in review) match slip rates and uplift patterns fairly well. Consequently, we incorporate the San Bernardino strand of the SAF, the San Gorgonio Pass Thrust and a portion of the Garnet Hill strand of the SAF into our semi-regional fault geometry. Because the full fault names are bulky, we drop "of the SAF" for the San Bernardino strand and Garnet Hill strand in the remainder of this report.

2 Completed Work

2.1 Dynamic Modeling Methods

We use the 3D dynamic rupture finite element method code FaultMod (*Barall*, 2009) for our dynamic faulting models. FaultMod takes the following as basic inputs: 3D mesh (i.e., discretized fault and material structure), friction law, stresses, nucleation location (hypocenter), material properties, model duration, and time stepping. Using these inputs, FaultMod solves for displacement at the nodes of the elements, stresses in the elements, and tractions at the fault element faces. In general, the calculations rely on Newton's second law of motion and Hooke's law, which provides the relationship between strain and stress (*Taylor*, 2005; *Mac Donald*, 2007; *Zhang et al*., 2009). The outputs are absolute normal and shear stresses, slip, slip rate, and particle (including ground) motion. The code has been validated through the Southern California Earthquake Center Code Validation Project (Harris et al., 2009).

Dynamic rupture models fully consider the time-varying interaction between motion, forces, and material properties, and thus are an approach well-suited to answer the questions of whether it is possible for rupture to propagate through the SGP. The method allows us to explore the effects of fault geometry and various stress field assumptions on slip distribution and rupture propagation paths over time (Aochi *et al*., 2000; Aagaard *et al*., 2004; Oglesby *et al*., 2003a; 2003b; Oglesby, 2005; Duan and Oglesby, 2007; Templeton, 2009; Lozos *et al*., 2011; Lozos *et al*., 2012).

We use the fault geometry used in quasi-static crustal deformation models of Herbert and Cooke (2012), Herbert et al. (2014), and Fattaruso (2014) to successfully match geologic slip rates and patterns of GPS velocities and uplift. This fault geometry is based on the Southern California Earthquake Center Community Fault model version 4 (Plesch, 2007), with small refinements introduced by Herbert and Cooke (2012), Herbert et al. (2014), and Fattaruso et al. (2014). We convert and slightly smooth the mesh from Herbert and Cooke (2012) and create the

model geometry in the csimsoft software toolkit Trelis, which is based on the CUBIT software from Sandia National Laboratories. We mesh the fault surfaces with 300 m triangular elements and the volumes with tetrahedra. Bias is implemented so that elements far from the faults are three times larger than elements around the faults, in order to keep the total number of elements small enough to be compatible with our current computing facilities. The meshed fault geometry is shown in Figure 2. While the mesh extends down to 35 km, we only allow the upper 20 km to rupture. We handle the junction line of the San Bernardino strand and the portions of the San Gorgonio Pass Thrust by removing a single line of nodes along that intersection, because in our method a fault node can only slip in a single direction, and thus there is ambiguity at fault intersections. For simplicity, when referring to the models, we break the fault geometry down into four sections: the San Bernardino strand (SB), the western portion of the San Gorgonio Pass Thrust (WSG), the eastern portion of the San Gorgonio Pass Thrust (ESG), and the Garnet Hill strand (GH). Breaking the fault geometry into these sections has no geologic significance; it is simply for referential ease when describing setup or results of the models.

Figure 2. Mesh Specifications. The faults are oriented northwest to southeast. The surface trace length of the SB, ESG, and GH combined is 123.3 km and the length of the WSG is 17.1 km. The rupturable depth of the mesh is set to 25 km, as marked on the mesh.

The two main variations we investigate with these models are the effects of the different stress field assumptions and different nucleation locations. For all models we use the slip weakening friction law (*Ida*, 1972) to isolate the effects of the stress assumptions without adding frictional complexity. The results of the models are divided into three main categories based on their initial stress inputs: Constant Tractions, Regional Stress, and Evolved Stress.

In the Constant Tractions models, the SB and GH are loaded in a purely strike-slip manner and the WSG and ESG fault portions, which strike oblique to this shear direction, have equally partitioned right-lateral strike-slip and thrust loading. There is precedence for abrupt changes in the orientation of the pre-stress field along modeled faults (e.g., Duan, 2010) and we employ the simplest assumptions with the Constant Tractions models for comparison with the more complex pre-stress assumptions of the other models. The tractions are considered constant because the initial shear along-strike traction value is the same for every element along the SB and GH, as is the initial normal traction value. Likewise, the WSG and ESG have the same initial shear along-strike and along-dip traction values. With constant frictional parameters, we back-calculate the magnitude of the initial constant shear and normal tractions assuming a 3 MPa

stress drop. Physical and computational parameters for the Constant Tractions models are listed in more detail in Table 1.

For the regional stress models, we use the orientation of the tectonic stress regime and the relative magnitude of the three principal stress axes (A_ϕ) of the SGP from Hardebeck and Hauksson (2001) as the inputs. We use the A_ϕ parameter as defined in Simpson (1997) to calculate ratios of initial stress end members for the range of $A_\phi = 1.5 – 2.3$, as determined for depths of 10 km within the SGP (*Hardebeck and Hauksson*, 2001). The lower end member of 1.5 represents a stronger strike-slip component because $A_\phi \approx 1$ indicates pure strike-slip. The upper member is 2.24, which has a higher compressive component because $A_\phi \approx 3$ indicates pure compression. We resolve two regional stress tensors for the end members onto the fault planes in FaultMod. Physical and computational parameters for the Regional Stress models are listed in Table 2. The difference in the frictional parameters between the Constant Tractions and Regional Stress models is due to the need to maintain strength ratios (or S values) that can facilitate rupture with the specified Constant Tractions. Das and Aki (1977) define the dimensionless quantity S as,

$$S = \frac{\tau_u - \tau_0}{\tau_0 - \tau_f} \quad (1)$$

where τ_u is the yield stress, τ_0 is the initial shear stress, and τ_f is the final traction. High S values indicate that a fault is far from failure and low values indicate a fault is favorable for rupture.

The models with Evolved Stresses use the stress outputs of quasi-static crustal deformation modeling from *Stern and Cooke* (2015) and *Stern* (2016). Because this approach utilizes a separate set of models and analysis, we describe this approach and findings in the following section of this report. The outputs from the evolved stress modeling are used as input to the dynamic models, and those results are discussed along with the other pre-stress conditions in section 2.3 of this report. We note that the details of the evolved stress modeling will appear in a separate peer-reviewed publication from the results of the dynamic models. For the sake of this USGS Final Report, however, we provide details of the quasi-static modeling of evolved stresses within the framework of the dynamic rupture study.

2.2 Estimation of evolved stress

In quasi-static crustal deformation modeling, long-term stressing rates are evaluated in a two-step back slip approach (e.g. *Marshall* et al., 2009). The first step finds the distribution of long-term steady-state fault slip compatible with applied plate velocities. The second step applies the steady-state fault slip below the locking depth to simulate interseismic loading. Following the approach of *Smith-Konter and Sandwell* (2006), likely shear traction distributions on the faults of this study are determined from the interseismic stressing rates using recurrence intervals and the time since the last earthquakes, as established in the literature. This method creates a set of pre-stress conditions that should provide a more realistic estimation of the heterogeneous pre-stress conditions along the faults in the SGP region than either constant tractions or a regional stress field (Figure 3).

2.2.1 Quasi-static crustal deformation

We use Poly3D, a quasi-static, three-dimensional Boundary Element Method code, to simulate deformation along the southern San Andreas Fault system. Poly3D solves the relevant equations of continuum mechanics to calculate stresses and displacements throughout the model [e.g. *Crouch and Starfield,* 1990; *Thomas*, 1993]. Faults are discretized into triangular elements of constant slip (no opening/closing is permitted) within a linear-elastic and otherwise

homogeneous half-space. In order to capture the tectonic setting of the San Gorgonio Pass, we simulate the active fault geometry of the southern San Andreas fault, the San Jacinto fault, and the Eastern California Shear Zone based on the Southern California Earthquake Center's Community Fault Model (CFM) version 4.0 [*Plesch* et al., 2007]. We include modifications to the CFM that serve to better represent the active fault geometry and match the geologic slip rates in the region assessed by *Beyer et al*. (in review).

We use a two-step modeling approach to estimate the interseismic stressing rates along the southern San Andreas fault. The first model simulates deformation over many earthquake cycles (steady state model) providing slip-rate information to an interseismic model that simulates the build-up of stress between earthquakes. In the steady state model, tectonic loading is prescribed far from the investigated faults at the base of the model; faults slip and interact in response to this loading. Using this approach, *Beyer et al*. (in review) compared the slip rate distribution from 5 plausible active fault configurations to geologic slip rate data. For this study, we use the slip rate distribution from *Beyer et al.* (in review) that best-fits the geologic data with inactive Mill Creek fault. *Beyer et al*. (in review) also tested each of the plausible fault configurations under a range of reasonable tectonic loading; for this study we use the mean slip rate from the different tectonic loadings. To simulate interseismic deformation, we prescribe this distribution of strike-slip rates to fault surfaces below 25 km and lock fault elements above 25 km depth. We use a depth of 25 km to ensure that our models produce reliable fault stresses to about 20 km depth that can be used within the dynamic rupture models. The abrupt transition from locked to slipping at the specified locking depth produces stresses that are unreliable within 5 km of this transition.

2.2.2. Method for estimating Evolved Stresses

The interseismic model determines stressing rates due to deep movement along active faults, which are used to calculate absolute shear stress along the fault segments of the southern San Andreas fault within the San Gorgonio Pass. To estimate absolute shear tractions on the fault, we assume complete coseismic stress drop during large ground-rupturing events. Following *Smith-Konter and Sandwell* [2006], we use the stressing rate information from the interseismic model and the time since last earthquake for each fault. In this approach, only large ground-rupturing events that are likely to be preserved in the paleoseismic record are considered. Complete stress drop is consistent with recent field measurements of low temperatures along recently ruptured fault surfaces, a result of a very low dynamic friction (e.g. *Carpenter*, 2012, *Fulton et al.,* 2013, *Li et al.,* 2015). The associate shear stress at any time in the earthquake cycle is

$$\tau = \dot{\tau} \cdot t \qquad (2)$$

where τ is the absolute shear stress, $\dot{\tau}$ is the shear stressing rate and t is time since last event. While we use this assumption to estimate absolute shear stress, we acknowledge that the shear stress evolution over several earthquake events is much more complex (e.g. *Matthews et al.* 2002; *Ellsworth et al*. 1999; *Molnar*, 1979) and not all events have complete stress drop. While the approach to calculate absolute stress is simplified, this distribution of shear stresses may affect dynamic rupture models and may provide more accurate initial conditions than resolving the remove loading onto the faults.

Recent earthquakes may also impact the stress state on nearby faults (e.g. *Harris and Simpson*, 1992, *Stein et al.,* 1992, *King et al.* ,1994; *Freed et al*., 2007).). For the faults within the San Gorgonio Pass, we consider the impact of the nearby 1992 Landers earthquake. The earthquake is simulated by applying slip distribution associated with the earthquake from (*Bryant,* 1992; *Bryant*, 1994; *Madden and Pollard*, 2012) to the model. All other faults in the

model are locked. The stress change due to the Lander's earthquake is summed with the evolved shear tractions calculated by equation 2 to produce the absolute shear tractions along the faults of the San Gorgonio Pass.

2.2.3 Shear stressing rate analysis

Maps of interseismic shear stressing rate along the southern San Andreas reveal how the fault geometry controls the stressing rate distribution. As expected along the primarily strike-slip San Andreas fault, right-lateral shear stressing rates are larger (maximum 12 kPa/yr) than the reverse-shear stressing rates (maximum ~3 kP/yr). Furthermore, faults parallel to the overall plate motion have greater dextral stressing rate. Right-lateral shear stressing rates are largest along the San Bernardino and Mission Creek strands of the SAF and decrease within the restraining bend of the San Gorgonio Pass region (Figure 3). The San Gorgonio Pass thrust has an undulating strike and small left-lateral shear stressing rates occur along some regions of the western San Gorgonio Pass thrust where the strike is less than ~265˚. As with dextral stressing rates, the reverse shear stressing rates increase with depth because deeper elements are closer to the deep slip that is applied to the interseismic model. The reverse-shear stressing rates are near to zero outside the bend and increase within the bend along north-dipping fault strands that strike obliquely to the plate motion and accommodate uplift (Figure 3).

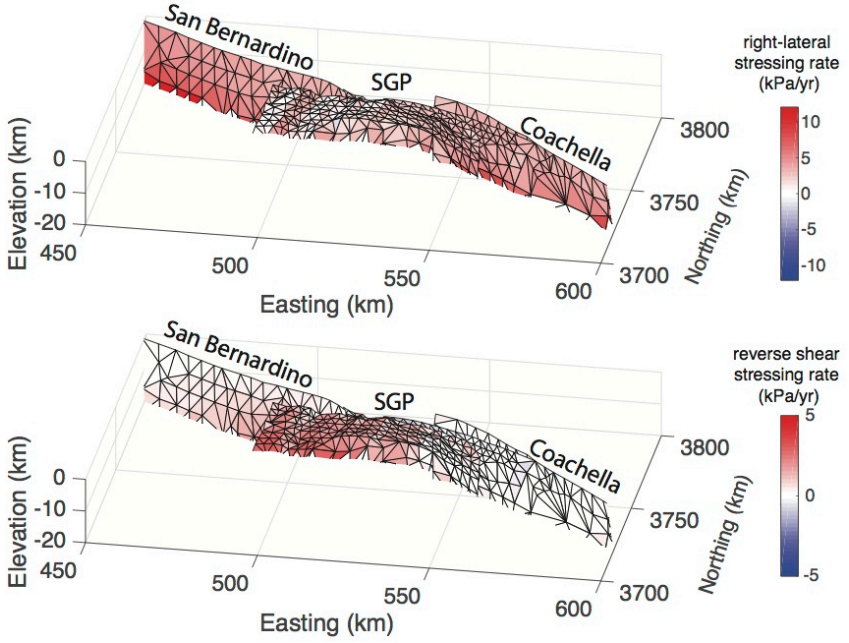

Figure 3. Dextral and reverse shear stressing rates along modeled surfaces representing the southern San Andreas fault through the San Gorgonio Pass region.

The first order pattern of shear stressing rate correlates with the orientation of the faults with regard to the regional stress. This suggests that resolving the tractions on the fault from the regional stress field may provide similar results as the stressing rate. Any differences between the two predictions owe to interaction among faults that is not considered in the resolved average regional stress distribution. To investigate the influence of fault interaction, we compare the interseismic shear stressing rates from the San Andreas and San Jacinto faults in our models with resolved tractions using $A\phi = 1.5$ described in the previous section of this report. Previous

models of the region have shown significant interaction between the San Andreas and San Jacinto faults (*Herbert et al*., 2012; *Fattaruso et al*, 2014), so we expand this analysis to include both of these faults.

The resolution of the remote stress tensor gives a dextral shear traction that depends on fault strike and is constant with depth. In contrast, the shear stress from the interseismic model increase with depth from zero at the Earth's surface to a maximum at 20 km near the deep interseismic loading of the fault system. To better correlate the two predictions, we apply a linear increase of dextral shear with depth to the resolved shear stresses and scale the values to match those from the interseismic model (Figure 4).

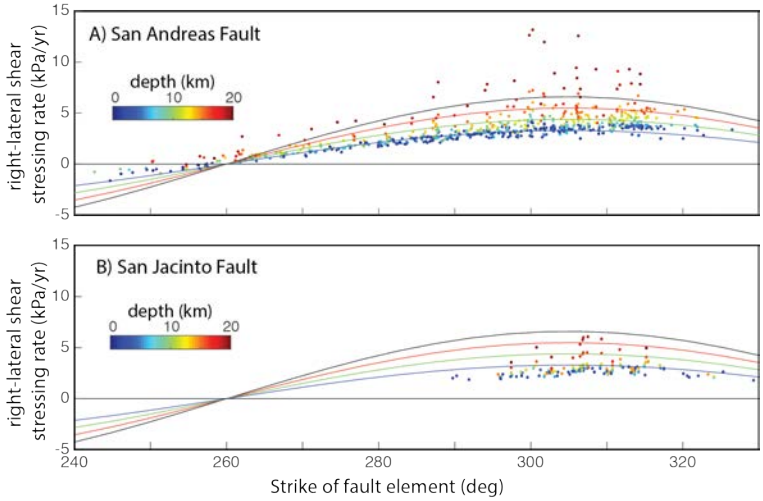

Figure 4: Dextral stressing rates versus fault strike of A) southern San Andreas fault and B) San Jacinto fault. Colors of symbol fill indicate depths of fault element and curves show the resolved shear stress scaled for linearly increasing depths. Shear stressing rates decrease away from the orientations of 305˚-310˚ and increases with depth.

The interseismic right-lateral shear stressing rates and the resolved shear tractions along the San Andreas fault show maximum around 305˚-315˚ with decreasing strike-shear stress as fault strike deviates from the orientation of maximum shear (Figure 4). Fault elements that strike more westerly than 260˚, such as along the San Gorgonio Pass thrust, display left-lateral shear. The relatively small variation in dextral stressing rates along the San Jacinto fault owes to the smaller variation strikes along this fault, which primarily parallel plate motion.

The match of the model results with the resolved stress is less consistent for the San Jacinto fault than for the San Andreas fault. The dextral stresses along elements of the San Jacinto fault have lesser value than elements of equivalent depth and strike along the San Andreas fault. For example, the red symbols are close to the red curves for the San Andreas plot but fall below the red curve for the San Jacinto plot (Figure 4

). This difference shows that resolving the dextral tractions from a uniform remote stress tensor will not provide the same distribution of shear stress as a model that considers fault interaction. We further demonstrate the difference in interseismic dextral stressing rate on similar striking portions of the San Andreas and San Jacinto faults by comparing the best-fitting surfaces through the data points between fault strikes of 290˚ and 320˚ (Figure 5). For similar fault strike and depth, the San Jacinto fault has lower right-lateral shear stressing rates than the San Andreas fault. This difference in strike-shear stressing rates owes to the interaction between the two faults

within the interseismic model. Estimating initial fault tractions using remote stress tensor cannot capture such fault interactions

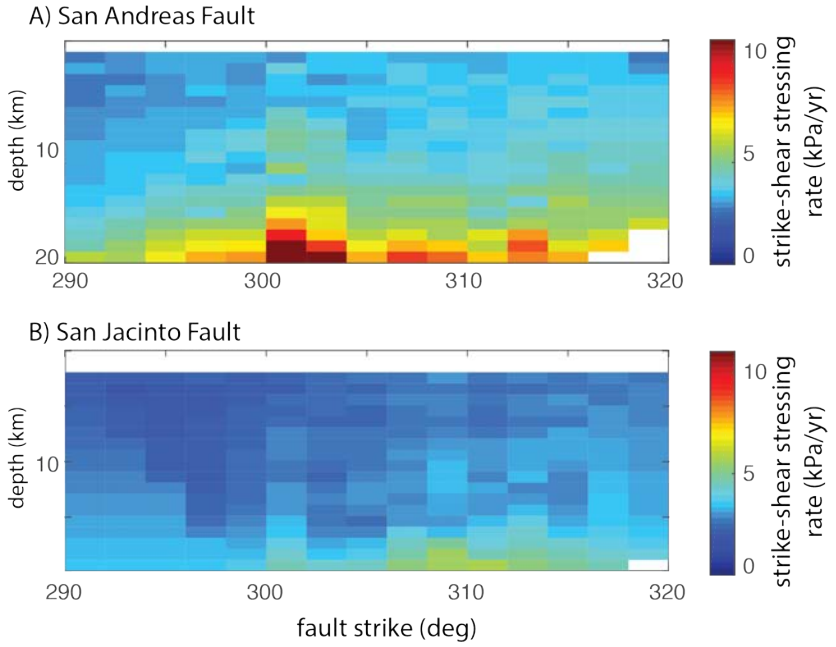

Figure 5: A gridded surface fit through the data points illustrates the different right-lateral stressing rates along the A) San Andreas and B) San Jacinto faults. For similar fault strike and depth, the San Jacinto fault has lower stressing rates

2.2.4 Evolved stress analysis

Paleoseismic data provide estimates for the year of the last rupture along active faults (e.g., *Biasi et al*., 2009). For the San Bernardino and Coachella segments, we use the compiled earthquake data from *Biasi et al.* (2009) (Table 2). Paleoseismic sites at Pitman Canyon, Plunge Creek, and Wrightwood provide a mean age of 204 years for the most recent earthquake year for the San Bernardino segment. The Thousand Palms Oasis and Indio sites provide mean time since last rupture of 616 years for the Mission Creek strand and the Coachella segment. For the San Gorgonio Pass thrust, Banning, and Garnet Hill strands of the SAF we use an earthquake rupture year of 1400 (*Heermance et al.,* 2014, *Yule et al.,* 2014). The Banning, Mission Creek strand and Coachella segments are not included in the dynamic rupture model but are included in the evolved shear stress analysis to provide context for the variation of tractions through the San Gorgonio Pass region.

	Paleoseismic Site(s)	Most recent EQ Year (AD)	Time since last event (yr)
San Bernardino	Pitman Canyon/Plunge Creek/Wrightwood (*Biasi et al.,*2009)	1812	204
Banning/SGPT/ Garnet Hill	Millard Canyon (*Heermance et al.,* 2014, *Yule et al*., 2014).	1400	616
Mission Creek/Coachella	1000 Palms/ Indio (*Biasi et al.,*2009)	1680	336

Table 2: Time since last event data from the year 2016 used to calculate absolute shear traction from the interseismic stressing rate.

Due to the variable time since last earthquake event across faults of the SGPr, the shear traction distribution along the fault surfaces (Figure 6) differs from the shear stressing rate distributions (Figure 3). Whereas dextral-shear stressing rates are lower along the north-dipping fault surfaces within the SGP restraining bend than on fault surfaces outside of the bend (Figure 3), the longer time since the last event along the north-dipping thrust faults increases the total right-lateral shear traction compared to other faults (Figure 6). Although the San Bernardino strand and the Coachella segment of the SAF have greater right-lateral stressing rates, the more recent rupture of these segments in the 1680 and 1812 events, which did not rupture through the restraining bend, reduced the accumulated stresses. The largest right-lateral shear tractions arise along the Banning and Garnet Hill strands of the SAF near the juncture with the Coachella segment of the SAF (Figure 3). Regions of large right-lateral shear traction also arise along portions of the San Gorgonio Pass thrust. The reverse shear tractions are greatest along the San Gorgonio Pass thrust within the restraining bend (Figure 3).

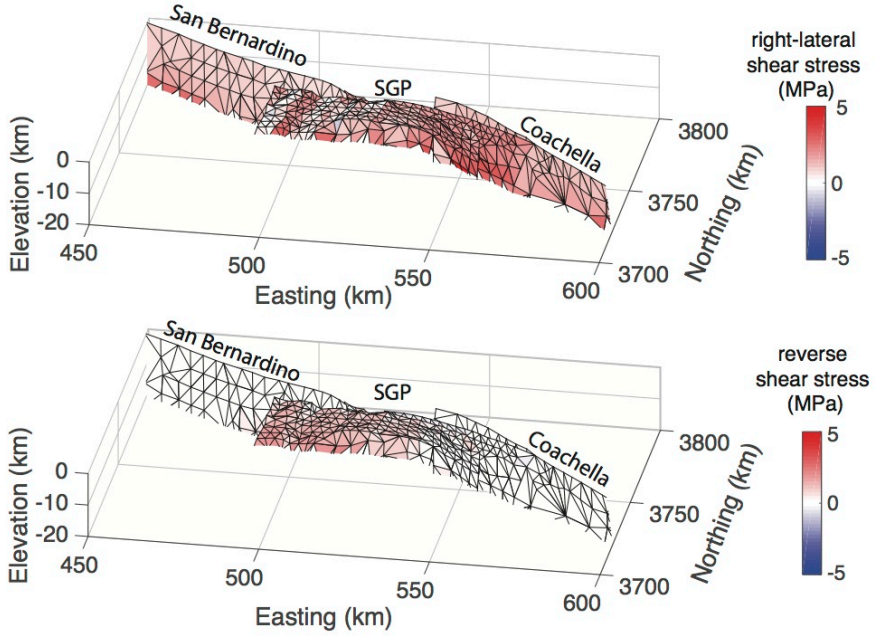

Figure 6: A) Right-lateral shear traction and B) reverse shear traction along modeled surfaces of the San Andreas fault through the San Gorgonio Pass region.

To include the impact of the 1992 Landers earthquake, we prescribe slip associated with the earthquake reported by *Bryant*, (1992), *Bryant* (1994) and *Madden and Pollard* (2012) onto fault surfaces within the model and examine the resulting static stress changes along the faults within the San Gorgonio Pass (Figure 7). Along the southern San Andreas fault, the Landers earthquake has the greatest impact within the restraining bend. The dextral tractions reach a maximum of ~0.3 MPa, along the San Gorgonio Pass thrust with sinistral tractions (negative) on the southern Garnet Hill and the Mission Creek strands of the SAF (Figure 7). Because all of these faults are loaded during the interseismic period with right-lateral shear stress, the Landers

rupture reduces total dextral traction along the Garnet Hill and Mission Creek strands and increases dextral shear accumulated on the San Gorgonio Pass thrust, presumably bringing this fault closer to failure. These static stress changes are small compared to the total accumulated tractions along these faults.

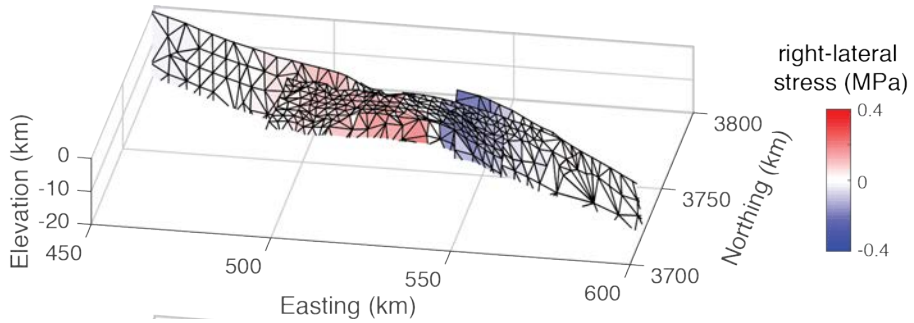

Figure 7. Static stress change along the San Andreas fault due to the simulated Landers rupture shows increased dextral loading of the San Gorgonio Pass thrust. Sinistral shear stresses show unloading of accumulated right-lateral shear on the Mission Creek and Garnet Hill strands of the SAF.

2.2.5 Implementation of evolved stresses in dynamic model

Due to the size difference between the elements used by Stern (2016) and the much smaller 300 m element sizes for the dynamic rupture models, we interpolate our traction values twice using a nearest neighbor approximation. The first interpolation is to eliminate NaN values in the shear tractions provided by Stern (2016), and the second round interpolates the values to our mesh designed in Trelis. A sample set of results is shown in Figure 8. While we use the shear traction output from Stern (2016), we do not use the normal traction output from those models because of uncertainties in how normal tractions accumulate over multiple earthquake cycles. Because normal tractions do not alternately accumulate and decrease in the same way as shear stresses over the earthquake cycle, these tractions can grow without bounds over long periods of normal stress accumulation. Our understanding of relaxation of normal stresses in the crust is not yet sufficient to allow us to use the normal stressing rates from the crustal deformation models to estimate normal tractions on the faults. Instead, we set the normal tractions by assuming a constant S value, or fault strength, along the entire fault geometry. The initial shear stress in Equation 1 is calculated from the values provided by Stern (2016). From the following relationships substituted into Equation 1, we can back-calculate σ_n, the normal traction:

$$\tau_u = \mu_s \sigma_n \quad (3)$$

$$\tau_f = \mu_d \sigma_n. \quad (4)$$

The values for the static μ_s and dynamic μ_d frictional parameters can be found in Table 3. The result is a distribution of normal traction that varies across the fault geometry. Although S is held constant to obtain the initial normal traction distribution, the dynamic stress interactions during the rupture simulation enable fault strength to vary temporally over the rupture duration.

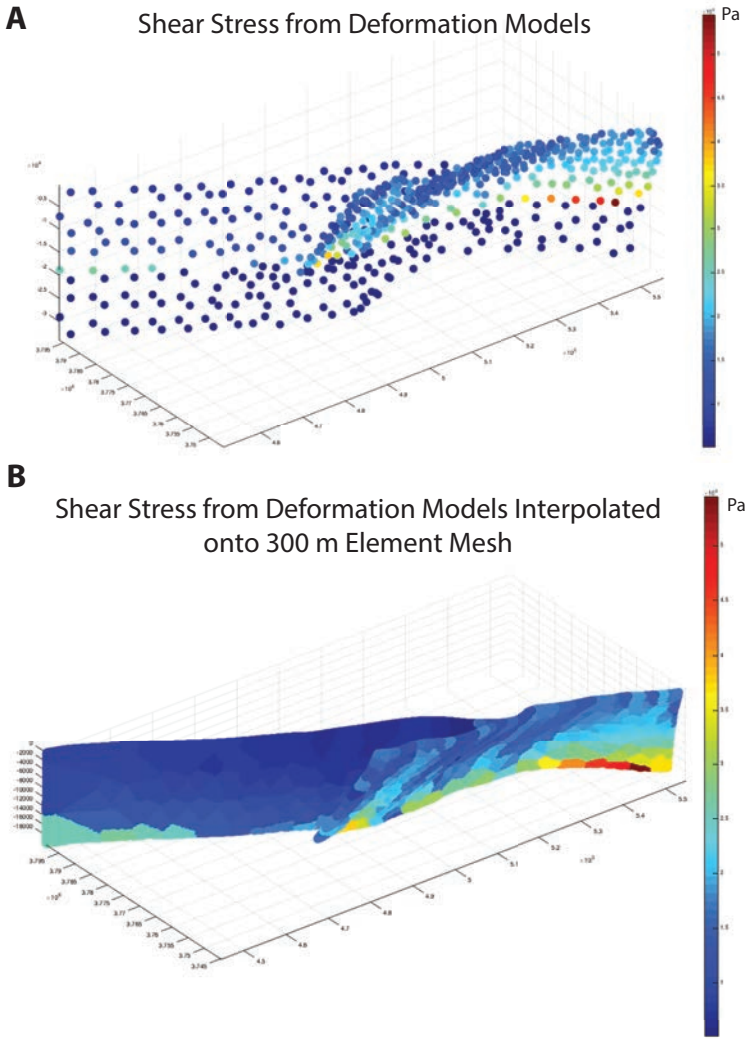

Figure 8. Plot of Initial Shear Tractions. (A) Net shear tractions from the deformation models, down to 35 km. This plot shows the coarseness of the initial shear traction distribution. (B) Interpolated shear traction down to the rupturable depth of 20 km. Darker blue colors indicate lower stress and red colors indicate relatively higher stress.

2.3 Results

Similar to Gilchrist (2015), our models have difficulty producing large ruptures, and in some cases are unable to rupture beyond the initial nucleation patch. The models show significant differences in rupture behavior between Constant Tractions and Regional Stress loading, most likely due to compatibility issues with the orientation of the pre-stress field and the complex fault geometry. Rupture behavior in the Evolved Stresses models is strongly controlled by the initial stress conditions, exhibited in the extreme variability in results from different nucleation locations.

2,3,1 Constant Tractions Models

We subdivide the Constant Tractions models into two groups: one that employs a linear gradient of normal compression down to 3 km, to simulate the decrease in absolute stress with lower lithostatic load near the surface, and one without a gradient in the normal stress. We find no significant difference in the results between these two groups. The four nucleation locations

that we tested with these models each produce distinct rupture patterns (Figure 9). Nucleation on the SB results in an earthquake that only ruptures the SB strand (Figure 9a). With nucleation on the ESG, rupture dies out quickly, after rupturing small amounts of the SB and GH (Figure 9b), which are more clearly visible when the color scale is over-saturated because the value is roughly 0.6 m of slip. The entirety of the ESG does not slip. Nucleation on the WSG leads to rupture propagation across to the ESG (Figure 4c), which is unsurprising because although these two portions are separated by a line of nodes removed along the intersection with the SB, these two portions have the same initial stress field orientation. With nucleation on the GH, rupture terminates on that fault and does not propagate through to the oblique ESG portion of the fault network.

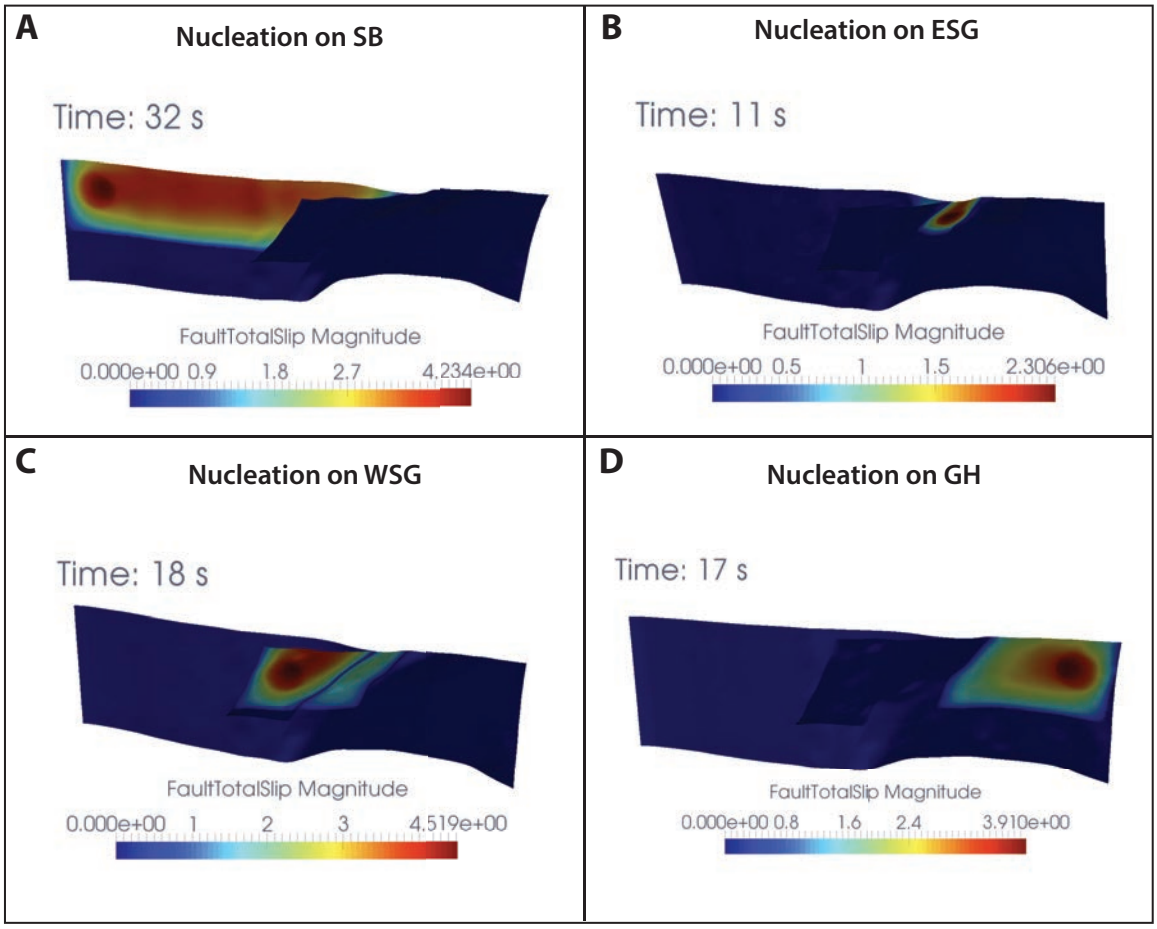

Figure 9. Summary Plot of Constant Tractions Models. These show the total slip plots at the end of the simulation for four different nucleation locations. (A) Nucleation on SB. (B) Nucleation on ESG. (C) Nucleation on WSG. (D) Nucleation on GH. Total slip magnitude is given in meters. These models with constant traction do not result in any through-going rupture scenarios.

2.3.2 Regional Stress Models

We test two end members of the relative magnitude of the three principal stress axes, $A_\phi = 1.5$ and $A_\phi = 2.24$, with the same nucleation locations employed in the Constant Tractions models. These stress values are depth-independent, and similar in scale to the Constant Tractions models. Unlike the Constant Tractions models, the stress field in these models does not have an abrupt transition in this location so we keep the nodes in the Regional Stress and Evolved Stresses models. For the both the Regional and Evolved Stresses, we only test three

nucleation locations—on the SB, WSG, and GH, because the ESG and GH are connected as part of the same fault mesh in these models.

The $A_\phi = 1.5$ resolved regional stress field is more favorable for rupture than the Constant Tractions stress field. In the $A_\phi = 1.5$ set of models, nucleation on the GH leads to a through-going rupture scenario (Figure 10). By 12 seconds, the rupture has crossed over to both the WSG and the SB (Figure 10b). At 25.5 seconds there is a semi-circular patch of the SB that experiences stress shadowing due to rupture on the WSG (Figure 10c). Slip on the WSG dynamically decreases the shear stress on the nearly parallel SB, creating this stress shadow. The rupture continues until nearly the entire SB slips, leaving only a fraction of the previous area within the stress shadow un-ruptured (Figure 10d). The magnitude of the total slip is smallest along the SB within the stress shadow created by slip along the WSG. All of the results for the Regional Stress models are summarized in Figure 11. The entire fault system ruptures when earthquakes are initiated on either the GH or the SB. With nucleation on the WSG, rupture dies out after the nucleation phase, indicating that this particular stress field does not facilitate rupture on the WSG. Results from the $A_\phi = 2.24$ stress field closely resemble those of the $A_\phi = 1.5$ stress field (Figure 6). The most notable difference between the $A_\phi = 1.5$ and $A_\phi = 2.24$ models is that in the latter, the stress shadowing effect between the SB and WSG portions of the fault system is slightly more pronounced, with a smaller total slip magnitude along the SB in response to slip on the WSG. This difference arises because in a more compressive stress regime, slip along the predominately strike-slip SB is less favorable and the oblique dynamic stresses along the WSG help to further decrease shear stress on portions of the SB.

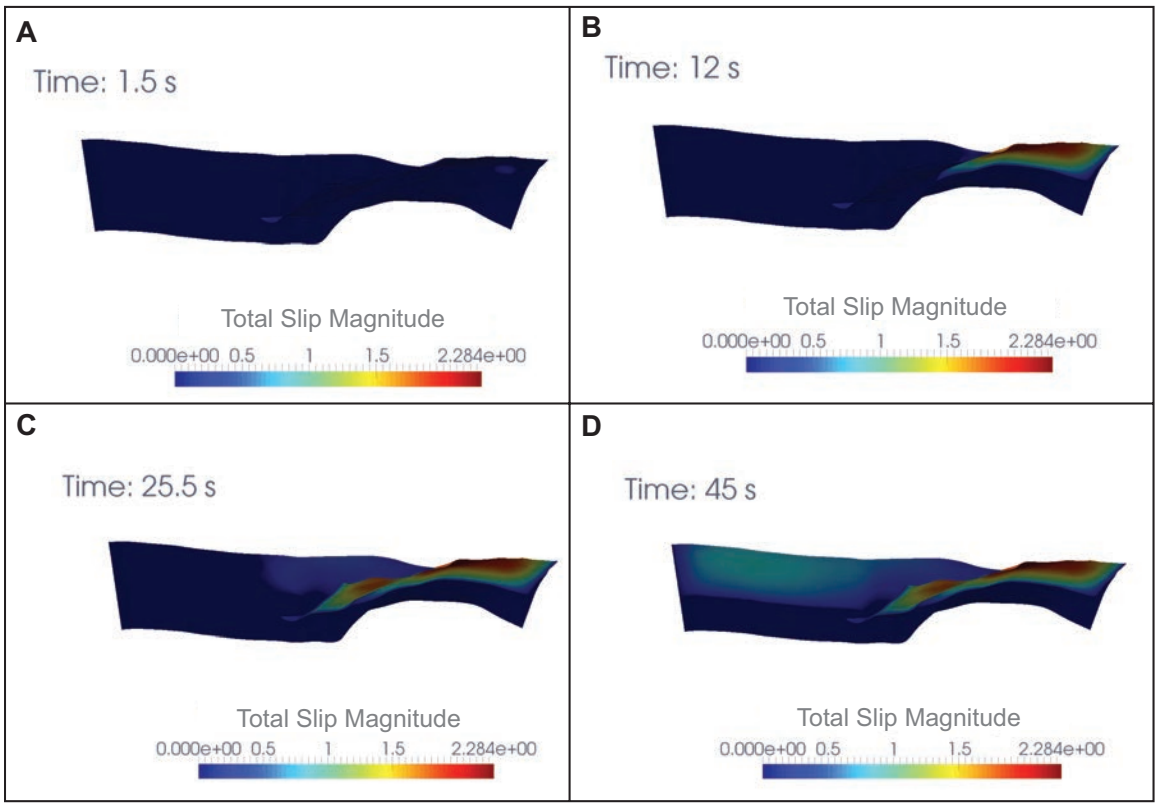

Figure 5. Example of Through-Going Rupture. These plots show the total slip at specific times during the simulation that employs a regional stress field with $A_\phi = 1.5$ and nucleation on the GH. Total slip magnitude is given in meters. Stress shadowing caused by slip on the WSG limits slip on the SB.

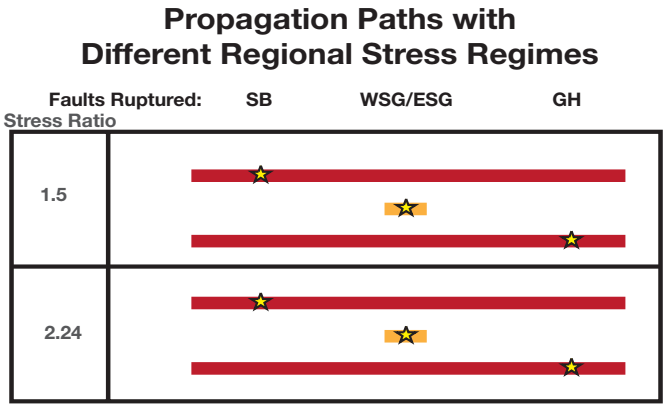

Figure 11. Summary of Regional Stress Model Results. Red bars indicate that a particular fault ruptured fully; orange bars indicate that only part of the fault slipped. Stars denote the fault on which rupture nucleated. For both stress ratios of $A_\phi = 1.5$ and $A_\phi = 2.24$, models that nucleated on the WSG failed to propagate out of the initial nucleation zone, while those that nucleated on the SB and GH resulted in multi fault rupture.

2.3.3 Evolved Stresses

This set of models, with nucleation locations matching those of the prior models, did not have straightforward results (summarized in Figure 12). Ruptures set to nucleate on the SB and WSG faults did not propagate outside of the initial nucleation zone, and the rupture that nucleated on the GH only propagated through part of the ESG. We attempted lowering the S value from 1.0 to 0.5, thereby lowering the variable normal traction, but the results did not qualitatively change. Given the relatively small shear stress magnitudes and variable distribution of the stresses, an estimate of the critical patch size for rupture nucleation (Day, 1982) implies a physically unreasonably large nucleation radius (on the order 30 km) would be needed to allow rupture to proceed spontaneously beyond the nucleation zone on the SB. Alternatively, we estimate that reducing the slip weakening distance d_0 (which is set essentially arbitrarily) by a factor of seven would promote spontaneous rupture. Using both S = 0.5 to generate the variable normal traction values and the smaller $d_0 = 0.086$ m, nucleating on the SB leads to a multi-fault rupture of the entire system, while nucleating on the GH yields results similar to the models that used S = 1.0 or S = 0.5 and a d_0 value of 0.6 m (Figure 12). Thus, we find that increasing or decreasing the (relatively unconstrained) slip weakening distance while using a highly heterogeneous stress field can have a very strong influence on the results.

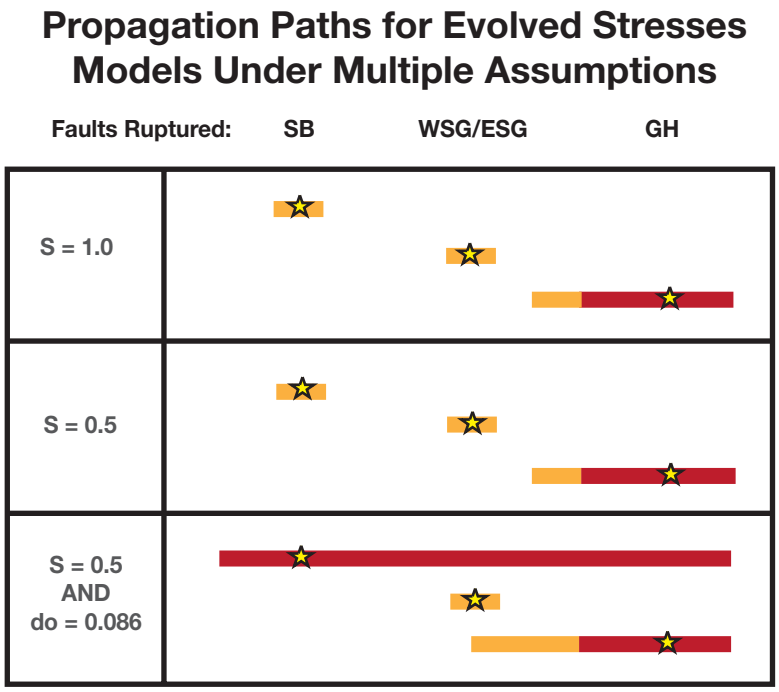

Figure 12. Summary of Evolved Stress Model Results. Red bars indicate that a particular fault ruptured fully; orange bars indicate that only part of the fault slipped. Stars denote the fault on which rupture nucleated. S values refer to the strength ratio used to generate the normal stresses (see Methods) and d_0 refers to the slip-weakening distance (m).

4. Discussion

In the case of the Constant Tractions models, the most likely cause for rupture terminating abruptly is changes in the orientation of the initial stress field. The abrupt rotation of the stress field from pure right-lateral strike-slip to oblique right-lateral and thrust at the modeled intersection between the San Bernardino and San Gorgonio Pass thrust likely causes rupture to stop at these segment boundaries because the pre-stress orientation is unfavorable with the complex fault geometry (Duan, 2010). In this case, the pre-stress orientation swamps the effect of the dynamic stresses, which would otherwise facilitate earthquake rupture propagation. However, if the crustal faults of the SGP have abrupt change in the orientation of the stress field, this supports suggestions that the SGP is a barrier for rupture and that through-going earthquakes are rare (Carena *et al.*, 2004; Langenheim et al., 2005). The effect of the shear stress orientation is so dominant that including, or not including, a linear gradient with the normal stresses appears to have almost no effect on the results.

The $A_\phi = 1.5$ Regional Stress models suggest that rupture directivity may play a key role in the viability of through-going rupture scenarios in the SGP. Nucleating along either the Garnet Hill or San Bernardino strands causes multi-fault rupture through the San Gorgonio Pass (Figure 6). However, nucleating from within the SGP does not lead to a multi-fault rupture scenario; rupture dies out shortly after nucleation in this somewhat unfavorable stress zone. This suggests that it is the dynamic stress changes from rupture propagation from elsewhere on the fault system, causing a significant build up of shear stress ahead of a rupture front coming from either the northwest or southeast, that allows the San Gorgonio Pass Fault Zone to rupture (in effect, allowing a "tunneling" of rupture through an otherwise less favorable region). This

directivity effect has been noted before in models of the North Anatolian Fault (Oglesby and Mai, 2012). The through-going scenario that starts in the southeastern part of the SGP falls in line with the hypothesis that a hypothetically large event rupturing through the SGP could start in Bombay Beach down by the Salton Sea and rupture through the San Gorgonio Pass (Olsen et al., 2006).

The results of the Evolved Stresses models with both the original d_0 and the scaled d_0 values suggest that some of the faults simply are not primed for failure with stresses evolved to 2016. This is obviously consistent with the observation that no ground rupturing earthquakes occurred in 2016. The pre-stress assumptions for these models take into consideration the time since a last event on these faults. For each of the different S value and d_0 assumptions, models that nucleate on the Garnet Hill strand rupture the Garnet Hill strand entirely and propagate partially along the San Gorgonio Pass Fault Zone. This suggests that the Garnet Hill strand is currently primed for failure, based on the loading caused by previous events and interseismic stress accumulation, and a more highly-stressed nucleation zone. Conversely, none of the Evolved Stresses models that nucleate on the San Gorgonio Pass thrust spontaneously rupture beyond the initial nucleation patch size. This suggests the San Gorgonio Pass thrust is not primed for failure. Events nucleating on the San Bernardino strand also die out in the initial nucleation patch with $d_0 = 0.6$ m. However, when we tune the d_0 value to allow rupture on the San Bernardino strand, rupture propagates across to the base of our artificially named WSG portion of the San Gorgonio Pass thrust. Rupture continues to propagate up-dip and southeastward, allowing shear stress to build up on the ESG portion as both the San Bernardino strand and the WSG portion slip. Eventually the entirety of the San Gorgonio Pass thrust and the Garnet Hill strand rupture as well, in an example of through-going rupture. Paleoseismicity indicates that it has been roughly 200 years since the San Bernardino strand failed in a large earthquake (McGill *et al*., 2002), which is relatively recent. Consequently, the evolved stress estimates have lower shear stress along the San Bernardino strand than other strands and this may explain why it is not primed for failure with a large d_0 value. Further investigation may be needed to see whether it is possible to fine-tune d_0 in a way that could produce a through-going rupture scenario with nucleation on the San Gorgonio Pass Fault Zone. Additionally, we could advance the investigation year beyond 2016 to see how many more years of loading would be required to produce a ground rupturing earthquake.

The results from the Evolved Stresses models also suggest that slip-weakening friction with a constant d_0 parameter may not be a compatible assumption with very heterogeneous initial stresses and geometry. There is large uncertainty about the d_0 parameter and its physical interpretation that makes it difficult to assess a reasonable numerical value for the parameter (Day, 1982). Given the sensitivities of this parameter with the evolved stress results, it may be necessary to explore the compatibility of time-weakening friction (Andrews, 1985) with highly variable initial stresses.

3. Conclusions

The results of dynamic rupture scenarios in the Western San Gorgonio are highly sensitive to assumptions about the initial stress distribution and frictional slip weakening parameter. Models that nucleate rupture on the San Bernardino strand and Garnet Hill strands are most sensitive to the pre-stress conditions. Nucleation on the San Bernardino strand results in single-fault rupture in the Constant Tractions models, through-going rupture in both sets of

Regional Stress models, and through-going rupture in the Evolved Stresses model with an extra-small slip weakening parameter under 2016 stress conditions. Models that nucleate on the Garnet Hill strand result in single-fault rupture in the Constant Tractions models, through-going rupture in both sets of Regional Stress models, and multi-fault (but not through-going) rupture in all of the Evolved Stresses models. The propensity of events nucleating on the Garnet Hill strand rupturing to other segments in the Evolved Stress model indicates that the estimated 2016 stresses may be great enough to initiate a ground rupturing earthquake in the San Gorgonio Pass. Models that nucleate slip on the San Gorgonio Pass thrust have the most consistent result, and demonstrate that it is difficult for ruptures starting within the San Gorgonio Pass to propagate outward towards either the San Bernardino strand or the Garnet Hill strand of the SAF.

Considering this summary of the results, we conclude that while not impossible, through-going rupture in the SGP is likely limited to specific stress conditions and dependent on nucleation location (which of course will itself be linked to the initial stress condition). Results from the Evolved Stresses models support the conclusions of Carena *et al*. (2004) that the SGP region can act as a barrier for through-going rupture, while the Regional Stress models show the possibility of occasional through-going rupture from earthquakes initiating from either the northwest or southeast (e.g. Carena *et al*., 2004; Olsen *et al*., 2006). These results are also consistent with those of Heermance and Yule (2017), who indicate that the SGP fault system has fewer earthquakes than the surrounding strands of the SAF, and likely rupture in events that break the SAF outside the Pass. The time since last event on the Coachella segment of the SAF, to the southwest of the Garnet Hill strand, is past its recurrence interval (~260 years), so we might expect the next earthquake in the region to initiate on the Coachella segment. The dynamic models of this study suggest that if such a rupture event propagates to the Garnet Hill strand, the rupture may pass through the San Gorgonio Pass. The difficulty with producing rupture along the San Gorgonio Pass thrust may indicate that our choice of SGP fault geometry strongly influences rupture at the inferred intersection of the San Bernardino strand and the San Gorgonio Pass thrust, regardless of the pre-stress conditions. We would need to conduct further investigations with alternate fault geometries to understand how strongly this fault geometry interpretation influences the results. Further investigation on pre-stress assumptions in dynamic rupture models is also necessary because it is clear that these stresses have a significant effect on rupture propagation paths and must be well understood in order to provide the seismological community with valuable results in geologically complex areas.

4 References

Aagaard, B.T., G. Anderson, and K.W. Hudnut (2004), Dynamic rupture modeling of the transition from thrust to strike-slip motion in the 2002 Denali Fault, Alaska, earthquake, *Bulletin of the Seismological Society of America*, *94*(6B), S190-S201.

Allen, C. R. (1957), San Andreas fault zone in San Gorgonio Pass, Southern California, *Geological Society of America Bulletin*, *68*, 315-350.

Andrews, D. J. (1976), Rupture velocity of plane strain shear cracks, *Journal of Geophysical Research*, *81*(32), 5679-5687.

Aochi, H., E. Fukuyama, and M. Matsu'ura (2000), Selectivity of spontaneous rupture propagation on a branched fault, *Geophysical Research Letters*, *27*(22), 3635-3638.

Barall, M. (2009), A grid-doubling technique for calculating dynamic three-dimensional spontaneous rupture on an earthquake fault, *Geophysical Journal International*, *178*, 845-859.

Beyer, Jennifer, Michele L. Cooke and Scott T. Marshall, in review. Sensitivity of deformation to activity along the Mill Creek and Mission Creek strands of the San Andreas fault. the *Geosphere special issue on Seismotectonics of the San Gorgonio Pass Region*

Biasi, G. P., & Weldon, R. J. (2009). San Andreas fault rupture scenarios from multiple paleoseismic records: Stringing pearls. Bulletin of the Seismological Society of America, 99(2A), 471-498.

Bryant, W. A. (1992), Surface rupture along the Johnson Valley, Homestead Valley, and related faults associated with the *M* 7.5 28 June 1992 Landers Earthquake, *Div. Mines Geol. Fault Eval. Rep. 234*, Calif. Dep. of Conserv. Sacramento, Calif.

Bryant, W. A. "Surface fault rupture along the Homestead Valley, Emerson, and related faults associated with the M 7.3 28 June 1992 Landers earthquake." *Fault Eval. Rep. FER* 239 (1994): 18.

Carpenter, B.M., D.M. Saffer, and C. Marone. Frictional properties and sliding stability of the San Andreas fault from deep drill coreGeology, August 2012, v. 40, p. 759-762, first published on June 15, 2012, doi:10.1130/G33007.1

Cooke, M. L., and L. C. Dair (2011), Simulating the recent evolution of the southern big bend of the San Andreas fault, Southern California, *Journal of Geophysical Research*, *116*, B04405, doi:04410.01029/02010JB007835.

Dair, L., and M. L. Cooke (2009), San Andreas fault geometry through the san Gorgonio Pass, California, *Geology*, *37*(2), 119-122.

Day, S. M. (1982), Three-dimensional simulation of spontaneous rupture: The effect of nonuniform prestress, *Bulletin of the Seismological Society of America*, *72*(6), 1881-1902.

Duan, B. (2010), Role of initial stress rotations in rupture dynamics and ground motion: A case study with implications for the Wenchuan earthquake, *J. Geophys. Res*., *115*, B05301, doi:10.1029/2009JB006750.

Duan, B., and D.D. Oglesby, 2007, Nonuniform prestress from prior earthquakes and the effect on dynamics of branched fault systems, *J. of Geophys. Res.*, *112*, B05308, doi:10.1029/2006JB004443.

Ellsworth, W. L., Matthews, M. V., Nadeau, R. M., Nishenko, S. P., Reasenberg, P. A., Simpson, R. W. "A physically-based earthquake recurrence model for estimation of long-term earthquake probabilities." *US Geol. Surv. Open-File Rept. 99* 522 (1999): 23.

Fattaruso, L., M.L. Cooke, R.J. Dorsey (2014), Sensitivity of uplift patterns to dip of the San Andreas fault in the Coachella Valley, California, *Geosphere*, *10*(6), 235–1246; doi:10.1130/GES01050.1.

Field, E.H., Biasi, G.P., Bird, P., Dawson, T.E., Felzer, K.R., Jackson, D.D., Johnson, K.M., Jordan, T.H., Madden, C., Michael, A.J., Milner, K.R., Page, M.T., Parsons, T., Powers, P.M., Shaw, B.E., Thatcher, W.R., Weldon, R.J., II, and Zeng, Y., 2013, Uniform California earthquake rupture forecast, version 3 (UCERF3)—The time-independent model: U.S. Geological Survey Open-File Report 2013–1165, 97 p., California Geological Survey Special Report 228, and Southern California Earthquake Center Publication 1792, http://pubs.usgs.gov/of/2013/1165/

Field, E.H., Biasi, G.P., Bird, P., Dawson, T.E., Felzer, K.R., Jackson, D.D., Johnson, K.M., Jordan, T.H., Madden, C., Michael, A.J., Milner, K.R., Page, M.T., Parsons, T., Powers, P.M., Shaw, B.E., Thatcher, W.R., Weldon, R.J. & Zeng, Y., 2015. Long-Term Time-Dependent Probabilities for the Third Uniform California Earthquake Rupture Forecast (UCERF3), *Bulletin of the Seismological Society of America,* 105**,** 511-543.

Freed, A. M., Ali, S.T.,and Bürgmann, R. "Evolution of stress in Southern California for the past 200 years from coseismic, postseismic and interseismic stress changes." Geophysical Journal International 169.3 (2007): 1164-1179.

Fulton P.M., et al., 2013, Low coseismic friction on the Tohoku-Oki fault determined from temperature measurements: Science, v. 342, p. 1214–1217, doi:10.1126/science.1243641

Gilchrist, J.J. (2015), Applications of Multi-Cycle Earthquake Simulations to Earthquake Hazard. UC Riverside: Geological Sciences. Retrieved from: http://escholarship.org/uc/item/6zv6912f.

Harris, Ruth A., and Simpson, Robert W. "Changes in static stress on southern California faults after the 1992 Landers earthquake." (1992): 251-254.

Herbert, J.W., and M.L. Cooke (2012), Sensitivity of the southern San Andreas fault system to tectonic bound- ary conditions and fault configurations, *Bull. of the Seis. Soc. of Am.*, *102*, 2046– 2062, doi: 10 .1785 /0120110316.

Herbert, J.W. et al. (2014), How much can off-fault deformation contribute to the slip rate discrepancy within the eastern California shear zone?, *Geology*, *42*, 71 – 74.

Heermance, Richard V. Geochronology of surfaces within the San Gorgonio Pass from radiocarbon, in-situ cosmogenic nuclides, and pedogenesis: implications for climate and tectonics since the mid – late Pleistocene. 2014 SCEC Annual Meeting.

Heermance, R.V., and D. Yule (2017), Holocene slip rates along the San Andreas Fault System in the San Gorgonio Pass and implications for large earthquakes in southern California, *Geophysical Research Letters*, 44, 5391-5400

Ida, Y. (1972), Cohesive force across the tip of a longitudinal-shear crack and Griffith's specific surface energy, *J. of Geophys. Res.*, *77*(20), 3796-3805.

Ikari, Matt J., Demian M. Saffer, and Chris Marone. "Frictional and hydrologic properties of clay-rich fault gouge." *Journal of Geophysical Research: Solid Earth* 114.B5 (2009).

Kame, N., J. R. Rice, and R. Dmowska (2003). Effects of pre-stress state and rupture velocity on dynamic fault branching, J. Geophys. Res. 108, no. 2265, doi 10.1029/2002JB002189

Kame, N., J. R. Rice, and R. Dmowska (2003), Effects of pre-stress state and rupture velocity on dynamic fault branching, *Journal of Geophysical Research*, *108*(B5), 2265, doi: 2210.1029/2002JB002189.

Kendrick, K. J., J. C. Matti, S. A. Mahan, G. P. Landis, and D. P. Miggins (2011), Depositional constraints on slip along the San Andreas fault within the eastern San Gorgonio Pass region, Southern California, *2011 SCEC Annual Meeting Program*, A-135.

Kendrick, K.J., J.C. Matti, and S. Mahan (2015), Late Quaternary slip history of the Mill Creek strand of the San Andreas fault in San Gorgonio Pass, southern California: The role of a subsidiary left-lateral fault in strand switching, Geol. Soc. of Am. Bull, 127, 825-849, doi:10.1130/B31101.1.

Kyriakopoulos, C., G. Funning, D.D. Oglesby, J.M. Fletcher, and K.J. Ryan (2015), The M7.2 2010 El-Mayor-Cucapah Earthquake: How much of the Complexity Can We Explain With Our Models?, *American Geophysical Union, Fall Meeting 2015*, abstract #T51H-02.

Li, H., Xue, L., Brodsky, E.E., Mori, J.J., Fulton, P.M., Wang, H., Kano, Y., Yun, K., Harris, R.N., Gong, Z. and Li, C., 2015. Long-term temperature records following the Mw 7.9 Wenchuan (China) earthquake are consistent with low friction. *Geology*, *43*(2), pp.163-166.

Lozos, J. C., D. D. Oglesby, B. Duan, and S. G. Wesnousky (2011), The effects of double fault bends on rupture propagation: a geometrical parameter study, *Bulletin of the Seismological Society of America*, *101*(1), 385-398.

Lozos, J. C., D. D. Oglesby, J. N. Brune, and K. B. Olsen (2012), Small intermediate fault segments can either aid or hinder rupture propagation at stepovers, *Geophysical Research Letters*, *39(*18), DOI: 10.1029/2012GL053005.

Madden, E.H., and Pollard, D.D. "Integration of Surface Slip and Aftershocks to Constrain the 3D Structure of faults Involved in the M 7.3 Landers earthquake, southern California." *Bulletin of the Seismological Society of America* 102.1 (2012): 321-342.

Marone, C., and Scholz, C.H. "The depth of seismic faulting and the upper transition from stable to unstable slip regimes." *Geophysical Research Letters* 15.6 (1988): 621-624.

Matthews, M. V., Ellsworth, W.L., and Reasenberg, P.A., "A Brownian model for recurrent earthquakes." *Bulletin of the Seismological Society of America* 92.6 (2002): 2233-2250

Matti, J. C., and D. M. Morton (1993), Paleogegraphic evolution of the San Andreas fault in Southern California: A reconstruction based on a new cross-fault correlation, in *The San Andreas fault system: Displacement, palinspastic reconstruction, and geologic evolution*, edited by R. E. Powell, R. E. I. Weldon and J. C. Matti, pp. 107-159, Geological Society of America.

Matti, J.C., B.F. Cox, C.M., Obi, R.E. Powell, M.E. Hinkle, Griscom, Andrew, and E.L. McHugh, (1982), Mineral resource potential of the Whitewater Wilderness Study Area, Riverside and San Bernardino Counties, California, *U.S. Geological Survey Miscellaneous Field Studies Map MF-1478*, scale 1:62,500.

Matti, J. C., D. M. Morton, and B. F. Cox (1985), Distribution and geologic relations of fault systems in the vicinity of the central Transverse Ranges, southern California, scale 1:250,000, *U.S. Geol. Surv. Open File Rep.*, *85-365*.

McGill S., Dergham S., Barton K., Berney-Ficklin T., Grant D., Hartling C., Hobart K., Minnich R., Rodriguez M., Runnerstrom E., Russell J., Schmoker K., Stumfall M., Townsend J., Williams J., (2002), Paleoseismology of the San Andreas fault at Plunge Creek, near San Bernardino, southern California. *Bull. Seismol. Soc. Am*. 92, 2803–2840.

Molnar, P. "Earthquake recurrence intervals and plate tectonics." *Bulletin of the Seismological Society of America* 69.1 (1979): 115-133.

Oglesby, D. D. (2005), The dynamics of strike-slip step-overs with linking dip-slip faults, *Bulletin of the Seismological Society of America*, *95*(5), 1604-1622.

Oglesby, D.D., S.M. Day, Y.-G. Li, and J.E. Vidale (2003a), The 1999 Hector Mine earthquake: the dynamics of a branched fault system, *Bulletin of the Seismological Society of America*, *93*(6), 2459-2476.

Oglesby, D.D., S.M. Day, and D.R.H. O'Connell (2003b), The dynamic and static interaction of two thrust faults: a case study with general implications, *Journal of Geophysical Research*, *108* (B10), 2489, doi:10.1029/2002JB002228.

Olsen, K. B., S. M. Day, J. B. Minster, Y. Cui, A. Chourasia, D. Okaya, P. Maechling, and T. Jordan (2008), TeraShake2: Spontaneous rupture simulations of M-w 7.7 earthquakes on

the southern San Andreas fault, *Bulletin of the Seismological Society of America*, *98*(3), 1162-1185.

Olsen, K. B., S. M. Day, J. B. Minster, Y. Cui, A. Chourasia, M. Faerman, R. Moore, P. Maechling, and T. Jordan (2006), Strong shaking in Los Angeles expected from southern San Andreas, *Geophysical Research Letters*, *33*, L07305, doi:07310.01029/02005GL025472.

Plesch, A., et al. (2007), Community Fault Model (CFM) for Southern California, *Bulletin of the Seismological Society of America*, *97*(6), 1793-1802.

Ramzan, S. (2012), Paleoseismic investigation of the San Gorgonio Pass fault zone near Cabazon, California, California State University, Northridge.

Scharer, K. M., D. Yule, L. R. Humbert, R. Witkowsky (2013), Implications for San Andreas Fault Ruptures Based on New Evidence from the Cabazon, CA Paleoseismic Site, San Gorgonio Pass Fault Zone, *American Geophysical Union, Fall Meeting 2013*, abstract #T43A-2622.

Smith-Konter, B., and Sandwell, D. "Stress evolution of the San Andreas fault system: Recurrence interval versus locking depth." *Geophysical Research Letters* 36.13 (2009).

Stein, R. S., King, G. C., & Lin, J. (1992). Change in failure stress on the southern San Andreas fault system caused by the 1992 magnitude= 7.4 Landers earthquake. *Science*, *258*(5086), 1328-1332.

Stern, A. and M. L. Cooke (2015), An approach for calculating absolute stress from stressing rate, *Southern California Earthquake Center, Annual Meeting 2014*, poster.

Stern, Aviel R. 2016. Fault interaction within restraining bend fault systems, MS thesis, University of Massachusetts, Amherst.

Templeton, E. L., H. S. Bhat, R. Dmowska, and J. R. Rice (2009), Dynamic rupture through a branched fault configuration at Yucca Mountain and resulting ground motions, *Bulletin of the Seismological Society of America, 100*(4), 1485-1497.

ten Brink, U., and Lin, J.(2004), Stress interaction between subduction earthquakes and forearc strike-slip faults: Modeling and application to the northern Caribbean plate boundary, *J. Geophys. Res.*,**109**, B12310, doi:10.1029/2004JB003031

Yule, D. (2009), The enigmatic San Gorgonio Pass, *Geology*, *37*(2), 191-192.

Yule, D., and K. E. Sieh (2003), Complexities of the San Andreas fault near San Gorgonio Pass: Implications for large earthquakes, *Journal of Geophysical Research*, *108*(B11), doi:10.1029/2001JB000451.

Yule, D., Scharer, K., Sieh, K., Wolff, L., McBurnett, P., Ramzan, S., Witkosky, R. and Desjarlais, I., 2014. Paleoseismology and slip rate of the San Andreas fault system at San Gorgonio Pass.

Table 1. Constant Traction Models: Physical and Computational Parameters

P-wave Velocity	**S-wave Velocity**	**Density**
5477 m/s	3162 m/s	2700 kg/m^3
Static Friction	**Dynamic Friction**	**Slip Weakening Distance**
0.84	0.42	0.6 m
Initial Shear Stress	**Initial Normal Stress**	**Nucleation Stress**
10 MPa	16.65 MPa	10.9 MPa
Small Element Size	**Large Element Size**	**Nucleation Radius**
300 m	900 m	5 km

Table 2. Regional Stress Models: Physical and Computational Parameters

P-wave Velocity	**S-wave Velocity**	**Density**
5477 m/s	3162 m/s	2700 kg/m^3
Static Friction	**Dynamic Friction Slip**	**Weakening Distance**
0.6	0.1	0.6 or 0.086 m
Small/Large Element Size	**Nucleation Radius**	**Nucleation Stress**
300/900 m	5 km	10% > Initial Stress

Stress Tensor Variation	σ_{00}	σ_{01}	σ_{02}	σ_{10}	σ_{11}	σ_{12}	σ_{20}	σ_{21}	σ_{22} **(MPa)**
$A_\phi = 1.5$	53	0	0	0	41.3	-3.76	0	-3.76	20.7
$A_\phi = 2.24$	69	0	0	0	42.4	-3.59	0	-3.59	22.6

Table 3. Evolved Stress Models: Physical and Computational Parameters

P-wave Velocity	**S-wave Velocity**	**Density**
5477 m/s	3162 m/s	2700 kg/m^3
Static Friction	**Dynamic Friction**	**Slip Weakening Distance**
0.6	0.1	0.6 or 0.086 m
Initial Shear Stress	**Initial Normal Stress**	**Nucleation Stress**
Variable (~1-6 MPa)	Variable (~1-14 MPa)	10% > Initial Stress
Small Element Size	**Large Element Size**	**Nucleation Radius**
300 m	900 m	5 km

PRESENTATIONS ON THIS WORK

Stern, Aviel R., Michele L Cooke, Jennifer L Beyer, Jennifer M Tarnowski, David D Oglesby, and Roby Douilly, 2016. Estimates of fault tractions in the San Gorgonio Pass region consider fault interaction, Southern California Earthquake Center Annual Meeting (Poster Presentation 058)

Stern, Aviel R. and Michele L. Cooke, 2015 An approach for calculating absolute stress from stressing rate, Southern California Earthquake Center Annual Meeting

Tarnowski, J.M., Oglesby, D.D. 2012. Preliminary dynamic models of potential earthquakes within the San Gorgonio Pass, California . Southern California Earthquake Center Annual Meeting. Palm Springs, CA

Tarnowski, J.M., Oglesby, D.D. 2012. Dynamic models of potential earthquakes in the San Gorgonio Pass, CA. American Geophysical Union Fall Meeting. San Francisco, CA.

Tarnowski, J.M., Oglesby, D.D., Kyriakopoulos, C. 2015. How Fault Geometry Affects Dynamic Rupture Models of Earthquakes in San Gorgonio Pass, CA. American Geophysical Union Fall Meeting. San Francisco, CA.

Tarnowski, J.M., Kyriakopoulos, C., Oglesby, D.D. 2016. The Effects of Pre-stress Assumptions on Dynamic Rupture with Complex Fault Geometry in the San Gorgonio Pass, CA Region. American Geophysical Union Fall Meeting. San Francisco, CA.

PUBLICATIONS ON THIS WORK

Beyer, Cooke, Stern and Oglesby, in preparation, Considering fault interaction in estimates of absolute stress along faults in the San Gorgonio Pass region, plan to submit to Geosphere special issue on the San Gorgonio Pass.

Stern, Aviel R. (2016), Fault interaction within restraining bend fault systems, MS thesis, University of Massachusetts, Amherst.

Tarnowski, J. M., Kyriakopoulos, C., Oglesby, D. D., Cooke, M. L., Beyer, J., and Stern, A., in preparation, Dynamic models of earthquakes in the San Gorgonio Pass region of the San Andreas Fault System, California; planned for submission to Geosphere special issue on the San Gorgonio Pass.

Tarnowski, J. M. (2017), The Effects of Dynamic Stress on Fault Interaction and Earthquake Triggering in the San Gorgonio Pass and San Jacinto, CA Regions, Ph.D. Dissertation, University of California, Riverside.